Title page

Biogenic nanoparticles from liquid and solid matrices: biochemical and biophysical properties of Extracellular Vesicles-enriched samples from human plasma and skeletal muscle tissue.

Authors: Valentina Mangolini[1,2], Annalisa Radeghieri[1,3], Simone Piva[4,5], Stefano Cattaneo[6], Marco Brucale[7,3], Francesco Valle[7,3], Arianna Balestri[8,3], Costanza Montis[8,3], Nicola Latronico[4,5,9], Paolo Bergese[1,3,10], Lucia Paolini[5,3]*.

Affiliations:

1. Dept. Molecular and Translational Medicine (DMMT), University of Brescia, Brescia, Italy.

2. IRCCS Fondazione Don Carlo Gnocchi ONLUS, Milano, Italy.

3. Center for Colloid and Surface Science, (CSGI), Sesto Fiorentino(FI), Italy.

4. ASST Spedali Civili di Brescia, Dept. of Emergency, Spedali Civili UniversityHospital, Brescia, Italy.

5. Dept. of Medical and Surgical Specialties, Radiological Sciences and Public Health (DSMC), University of Brescia, Brescia, Italy.

6. ASST Spedali Civili di Brescia, Dept. Orthopedyand Traumatology.

7. Consiglio Nazionale delle Ricerche, Istituto per lo Studio dei Materiali Nanostrutturati, Bologna, Italy.

8.Dept. of Chemistry “Ugo Schiff”, University of Firenze, Firenze, Italy.

9. “Alessandra BONO” University Research Center on LOng Term Outcome (LOTO) in Survivors of Critical Illness, University of Brescia, Italy

10. IRIB - Institute for Research and Biomedical Innovation of CNR, Palermo Italy.

*Corresponding author: Lucia Paolini

e-mail address: lucia.paolini@unibs.it

Postal address: Department of Medical and Surgical Specialties, Radiological Sciences and Public Health, University of Brescia. Viale Europa, 11, 25123, Brescia, Italy.

Phone number: +39 030 3717543

Financial Support and Sponsorship

This work was supported by the Italian Ministry of Health (Ministero della Salute) through the Ricerca Finalizzata (RF) "Theory enhancing" grant: ID project RF-2021-12375279 and "Alessandra Bono" Foundation;

Conflicts of Interest

The authors declare no conflicts of interest.

Word count for abstract: 149;

Manuscript word count (including body text and figure legends, but excluding abstract, title page, and references): 5523.

Number of references: 53

Number of figures/tables: 8

ABSTRACT:

The majority of studies on extracellular vesicles (EVs) focused on samples isolated from liquid matrices, such as cell culture media and blood, due to their accessibility. However, recent research highlights the emerging roles of EVs derived from solid tissues, including the brain, muscles and tumors. Investigating EVs from the extracellular matrix of solid tissues offers insights into their microenvironment and potential biological influences on surrounding cells. This study presents a method for comparing EV-enriched samples from solid (human skeletal muscle biopsy) and liquid (plasma) matrices, addressing technical challenges and minimizing biases in separation techniques. By employing optimized protocols and advanced analytical techniques, the study reveals

differences in biochemical composition, nanomechanical properties, particle yield, size distribution, and colloidal stability between human muscle and plasma EVs. Understanding these distinctions may contribute to the development of novel diagnostic assays for muscular pathologies and shed light on EVs' roles in diverse tissue environments.

KEYWORDS

Liquid and solid matrix, Extracellular vesicles, Skeletal muscle tissue, Plasma, Biochemical and biophysical properties.

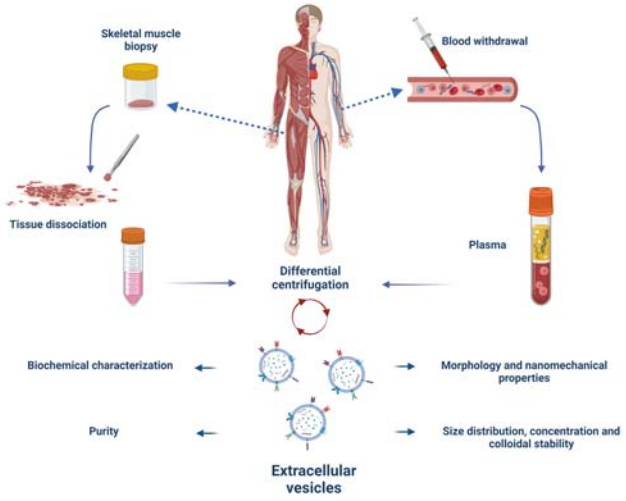

Graphical abstract: Extracellular vesicles (EVs) studies have primarily focused on liquid matrices like cell culture media and blood. However, emerging research highlights the importance of investigating EVs from solid tissues such as the brain, muscles, liver, and tumors. This study introduces a method to compare EVs-enriched samples from solid (human skeletal muscle) and liquid (plasma) matrices, addressing technical challenges and minimizing biases in separation techniques. Utilizing standardized protocols and advanced analytical methods, the research reveals differences in biochemical composition and biophysical properties between muscle and plasma EVs. Created with BioRender.com

Manuscript text

BACKGROUND

The majority of studies on EVs conducted thus far have mainly focused on EVs isolated from liquid matrices such as cell culture media, blood, and urine. This is ascribable to the fact that these samples are readily available and can be processed using established separation techniques[1]. As a result, our understanding of EVs has been limited to those found in these particular matrices.

In the latest years, the important roles of EVs in solid tissues[2,3], including human and non-human brains[4–9], cardiac and skeletal muscles[10,11], liver[12,13], adipose tissue[14,15] and several tumors[16–18], are emerging.

Studying solid tissue EVs is expected to offer a glimpse into the EVs in the microenvironment where they are released. Moreover, it provides the potential to comprehend the mechanisms through which EVs, released in the extracellular matrix of a tissue, exert a biological influence on their cellular targets, which may be located in various organs. By investigating solid tissue EVs, we can gain insights into the complex interplay between EVs and their surrounding environment, shedding light on the underlying processes and effects they have on cells.

This increases the possibility to find specific signatures of pathological conditions within organs. By analyzing the distinct profiles of tissue-EV associated with various diseases, researchers can uncover biomarkers that serve as diagnostic indicators. This knowledge could aid in early disease detection but also provides a basis for developing novel liquid biopsy assays[18,19] using blood or other biological fluids.

However, this perspective is at its infancy due to technical challenges[3] and the lack of rigorous approaches that allow comparing EVs from solid and liquid tissues, minimizing bias due to different separation techniques and highlighting differences due to the EV microenvironments.

A variety of techniques for EV separation is flourishing both for liquid and solid matrices. Common techniques applied to separate EVs from liquid matrices imply several combinations of differential (ultra)centrifugation, density gradient, size exclusion chromatography, fluid-flow based separation, affinity-based separation[1], and microfluidics techniques[20]. Separation of EVs from solid tissues usually involves tissue homogenization or tissue digestion with different enzymes followed by differential (ultra)centrifugation, filtration[2] and density gradients[3].

However, it has been demonstrated that different isolation methods can modify EV characteristics in terms of physical properties[21] (i.e. number density, size distribution, purity from exogenous contaminants) and biological activity[22,23]. Separation procedures can affect EV functionality both *in vitro*[24] and *in vivo*[23] and this is due to not only to intrinsic EV-properties, but also to the presence of EV co-isolates[25] and EV protein corona[26].

Furthermore, the exploration of how the biochemical and biophysical properties of EVs may vary between those present in the tissue environment and those circulating remains poorly investigated.

In order to investigate these points, we have chosen to analyze EVs from solid and liquid matrices: human skeletal muscle (SkM) and human plasma derived from blood. These samples have a great clinical relevance: SkM is not only the largest organ in the human body, playing a central role in whole-body energy metabolism, but also acts as a secretory organ, producing and releasing hundreds of products, including myokines and EVs (SkM-EVs) that can have autocrine, paracrine, and endocrine effects[10,11,27]. Plasma is the most studied source of EVs from bio-fluids[1].

To minimize modifications induced by differences in the separation process we standardized the procedure to the greatest practicable extent. Indeed, SkM-nanoparticles were released from the extracellular matrix in a liquid phase, using mechanical and enzymatic dissociation. EVs from tissue and plasma were, then, enriched using a consistent protocol involving serial ultra-centrifugations and discontinuous sucrose gradient.

We, then, characterized the preparations using orthogonal collective and single-particle analysis technique, dissecting sample characteristics at multi-scale levels: from the molecular scale (immunoassays to define their biochemical composition), to the meso-scale (determining samples colloidal properties in terms of purity from exogenous proteins, nano-mechanical features, concentration, size distribution and stability).

This allowed to compare "on a common reference" biochemical and biophysical properties of EVs secreted from cells forming the SkM and released in the interstitial space[4,6,10,17] of the tissues and EVs present in plasma, the intercellular matrix of blood, highlight specific characteristics.

Studies in this direction might be useful to develop novel, non-invasive diagnostic and monitoring assays for muscular pathologies including hereditary diseases such as metabolic myopathies, dystrophic myopathies or acquired conditions as Intensive-care acquired weakness in critically ill patients with sepsis[28,29].

METHODS

All data were acquired and described following the MIRABEL[30] and MISEV 2018[1] international guidelines. We have submitted all relevant data of EV samples to the EV-TRACK[31] database (EV-TRACK ID: EV240003) and MIBlood-EV[32] (see Supplementary Fig.1)

Subject Recruitment and Sample Collection

In this study, 5 plasma samples and 5 skeletal muscle (SkM) tissue biopsies were obtained from subjects hospitalized in the Intensive Care Unit (n=3) and Orthopedic ward (n=2) of the Spedali Civili University Hospital in Brescia, Italy. The Ethics Committee of Brescia approved the study in adherence with the Declaration of Helsinki and Good Clinical Practice (Protocol number 34 68). All traceable identifiers were removed before analysis to protect patient confidentiality; all samples were analyzed anonymously. Written informed consent was obtained from the patient before the collection of samples. The subjects were all male, with an age range of 53-75 years (average age

64,6 y/o). Both blood and SkM tissue biopsies were collected at the same time and processed within 30 minutes from the withdrawal.

Plasma was obtained as previously described from peripheral blood samples in EDTA[33]. Blood was collected through a peripheral venous catheter in one of the main venous trunks of the forearm and SkM tissue was collected from quadriceps femoris. See Supplementary Materials for more details.

Enrichment of EVs from human plasma

Plasma EVs were isolated through serial ultra-centrifugation and discontinuous sucrose gradient (DSG). All steps were performed at 4°C. Briefly, 1 ml plasma was centrifuged at 300 x g for 10 min. Supernatant (1 ml) was transferred to a new tube and centrifuged at 2,000 x g for 20 min. Supernatant (1 ml) was transferred to a new tube and centrifuged at 16,500 x g for 20 min and finally supernatant was transferred to an appropriate tube and centrifuged at 118,000 x g for 2h and 30 min. The 16,500 x g centrifugation step allows sedimentation of Plasma 16k sample, while the 118,000 x g ultracentrifugation step allow sedimentation of Plasma 118k sample.

DSG was carried out as follows: Plasma 16k and Plasma 118k pellets, obtained as described above, were further processed adapting the protocols developed in previous studies[26,33]. Briefly, Plasma 16k or Plasma 118k samples were re□suspended in 1,000 μl buffer A (10 mM Tris□HCl 250 mM sucrose, pH 7.4), loaded on top of a discontinuous sucrose gradient 15% (600 μl), 20, 25, 30, 40, 60, 65% (400 μl), 70% (800 μl) sucrose in 10 mM Tris□HCl, pH 7.4) and centrifuged at 230,000 x g for 16 h. For Western blot (WB) analysis of fractions 1-12 (250 μl) were precipitated by incubation with 10% trichloracetic acid for 4 h as described in Paolini et al.[34]. For all the other analyses, fractions from 6 to 9 (750 μl each) were ultracentrifuged and resupended in 100 μl HPLC water and aliquoted for further analyses. See Supplementary Materials for more details.

Enrichment of EVs from human SkM tissue

EVs were isolated from human SkM tissue after mechanical and enzymatic dissociation, as previously described[17] with some modifications. Frozen tissue was thawed 2 min at r.t., washed one with cold PBS 1x and weighted (5 samples, mean 0.89 gr). Tissue was transferred in a 100 mm dish with cold RPMI (medium/tissue ratio: 1ml RPMI/ 0.2 gr tissue) and gently cut into small pieces (2x2x2mm) with a scalpel. Tissue pieces were transferred in a 6-well plate with 0.2 gr of SkM tissue each well. RPMI medium was added to each well to reach 2 ml of total medium. SkM tissue was inoculated with DNase (40U/ml final concentration) and collagenase D (2mg/ml final concentration) at 37°C for 30 minutes in gently rotation (78 rpm). Medium derived after the enzymatic dissociation was filtered in a 0,70 µm pore strain in order to eliminate the largest debris. The filtrate was used for EV-enrichment through serial ultra-centrifugation and DSG as described for plasma.

Tissue filtrate was centrifuged at 300 x g for 10 min. Supernatant was transferred to a new tube and centrifuged at 2,000 x g for 20 min. Again, supernatant was transferred to a new tube and centrifuged at 16,500 x g for 20 min in order to obtain Tissue 16K preparation. Finally, supernatant was ultracentrifuged at 118,000 x g for 2 h and 30 min to get Tissue 118K preparation. All centrifugation steps were performed at 4°C.

DSG: Tissue 16k and Tissue 118k pellet obtained were treated as described for plasma preparations. For WB analysis of gradient fractions see section above.

SkM tissue homogenate was obtained from SkM tissue before (THB) and after the mechanical and enzymatic dissociation (TH). See Supplementary Materials for more details.

SDS-PAGE and WB analysis

SDS−PAGE and WB were performed by standard procedures[35,36] on total plasma or tissue homogenate (30 µg, protein content determined by Bradford assay) and sucrose density gradient fractions from 1 to 12 (30 µl of each fraction were loaded on a acrylamide–bisacrylamide, 12.5%

gel). Samples were electrophoresed and analyzed by WB with the antibodies described in the text. See Supplemental Material for more details.

COlorimetric NANoplasmonic (CONAN) assay

The EV-enriched preparations (DSG fractions 6-9) were checked for purity from protein contaminants using the COlorimetric NANoplasmonic (CONAN) assay[37,38]. EVs were resuspended in 100 µl of HPLC water. Two microlitres of EV solution at serial dilutions in HPLC water (1:1, 2µl of starting sample – 1:10, 2 µl of sample diluted in HPLC H_2O – 1:100, 2 µl of sample diluted in HPLC water) were resuspended in 23 µl of water, mixed with 50 µl of gold nanoparticles 6 nM and 25 µl of PBS. The result of the assay was collected on Ensight Multi Mode Reader (Perkin Elmer). Measurements were performed for each sample in triplicate.

Bicinchoninic acid (BCA) and Bradford assay

Protein concentrations of samples (fractions 6-9) were determined with a Pierce™ BCA Protein Assay Kit (ThermoFisher, Rockford, USA), and Bradford assay (Biorad) following the manufacturer's instructions.

Atomic Force Microscopy (AFM) analysis

Quantitative AFM morphometry was performed as described elsewhere[39,40]. Five µL aliquots from samples were deposited on glass coverslips previously functionalized with 0.01 mg/mL poly-L-lysine and left to adsorb for 60’ at 4°C. Aliquots were progressively diluted up to 200x in successive depositions in order to maximise the surface density of isolated particles. Imaging was performed in ultrapure water at room temperature on a Bruker Multimode8 AFM equipped with a Nanoscope V controller, a sealed fluid cell and a type JV piezoelectric scanner using Bruker ScanAsystFluid+ probes. Background subtraction was performed using Gwyddion[41] 2.61. Quantitative morphometry was performed with custom Python scripts to recover the surface contact

angle (CA) and equivalent solution diameter (D) of several hundred individual objects for each sample. The relative particle concentrations of samples were estimated as described in Supplementary section.

Nanotracking particle analysis (NTA)

Pellets from 6 to 9 sucrose fractions obtained from both plasma and human SkM tissue were pooled together, resuspended in 100 µl of sterile HPLC water and for the characterization by Nanoparticles Tracking Analysis (NTA) using a NanoSight NS300 system (Malvern, Panalytical LTD, Malvern, UK) to evaluate the concentration and size distribution of EVs. See Supplemental Material for more details.

Dynamic light scattering (DLS) analysis and zeta potential measurement

DLS at $\theta = 90°$ and zeta potential measurements were performed using a Brookhaven Instrument 90 Plus (Brookhaven Instruments Corporation, Holtsville, NY). For DLS, each measurement was an average of four replicates of 1 minute each. The autocorrelation functions were analysed by Laplace inversion using the CONTIN algorithm, allowing an estimate of the particles size distribution. Zeta potentials were obtained from the electrophoretic mobility u, according to the Helmholtz-Smoluchowski equation: $\zeta = (\eta/\varepsilon) \times u$ where η is the viscosity of the medium and ε is the dielectric permittivity of the dispersing medium. The zeta potential values are given as the average of ten measurements, performed in water.

Statistical analysis.

Significant differences among datasets were determined with Student's t-test (Graph Pad). P values of less than 0.05 were considered statistically significant with $^{**}p < 0.01$ $^{***}p < 0.001$ and $^{****}p < 0.0001$. Values were shown as mean ± standard error of the mean (SEM) of at least 3 experiments.

RESULTS AND DISCUSSION

Combined protocol for the enrichment of nanoparticles from human plasma and SkM tissue biopsies

Peripheral blood and SkM tissue biopsies were collected from 5 subjects. Blood was processed as described in Methods section to obtain plasma. SkM tissue was washed twice in cold solution NaCl 0.9% and sample tube was snap-frozen in liquid nitrogen. Both plasma and SkM tissue were stored at -80°C. Then, Plasma and SkM tissue biopsies were processed with a newly developed combined protocol (Figure 1).

SkM biopsy (mean weight 0.89 gr) was thawed and washed with cold PBS. The biopsy was then incubated in RPMI medium and processed through gentle mechanical and enzymatic dissociation with DNase and Collagenase for 30 min at 37°C. This process allowed to release nanoparticles embedded in the interstitial space surrounding tissue cells and to diffuse them in the media during the procedure[17]. The media containing SkM-EVs was filtered through a 70 μm pore cell strainer in order to eliminate the largest tissue debris. At this stage the same protocol for the EV isolation from plasma and SkM was used. The SkM filtrate and 1ml of plasma were centrifuged at 300g for 10 min, the supernatant (SN), collected without disturbing the pellet, was centrifuged at 2,000g for 30 min. Then, the subsequent SN was centrifuged at 16,500g for 20 min. The subsequent pellet is referred in the text as the Plasma or Tissue 16k subpopulations. Finally, the SN obtained after the 16,500g centrifugation was centrifuged at 118,000g for 2h 30 min to obtain pellets referred in the text as Plasma or Tissue 118k subpopulations.

It is recognized that pellets derived from both 16k and 118k Plasma and Tissue are composed by a complex mixture of different biogenic nanoparticles[42]: extracellular particles (EP- i.e. extracellular vesicles), non-vesicular extracellular particles (NVEP- i.e. lipoproteins, exomeres[43]), cellular and tissue small debris. In order to refine the separation of EPs, all four samples were loaded, separately, on top of a discontinuous sucrose gradient (DSG) and centrifuged at 230,000g for 16h.

This allows the separation of different nanoparticles both for their size and density[26,33,44,45]. Twelve fractions of equal volume (400 µl) were collected, processed as described in Methods section and analyzed as further described.

Selection of Plasma and Tissue-EV positive fractions by biochemical characterization

WB analysis was conducted for the biochemical characterization of the twelve fractions deriving from the processing of the Plasma 16k, Plasma 118k, Tissue 16k and Tissue 118k pellets by DSG. This allowed to determine the gradient fractions enriched in EVs and fractions enriched in NEVPs markers. Different proteins were selected according to MISEV 2018 guidelines[1] and recent studies[46]: EV markers (tetraspannins CD63, CD81; protein involved in the vesicular trafficking such as Flotillin1; single-pass transmembrane protein such as ADAM10; component of the ESCRT□I complex such as TSG101); lipoproteins markers (ApoB marker of Low-density and Very-Low density Lipoproteins -LDL and VLDL; APOA1 marker of High Density Lipoprotein-HDL); SkM cell and SkM-EVs[10,11] markers (Caveolin-3 and Beta-enolase); markers of contaminants (hemoglobin A for blood; Fatty Acid binding protein (FABP) for adipose tissue[47]; GM130 and Calnexin for intracellular compartments: the Golgi network and the endoplasmic reticulum respectively).

As shown in Fig. 2, fractions 4 and 5 (red box, corresponding to a density of 1.09-1.11 g/cm^3) resulted enriched in HDL marker ApoA1 both in Plasma 16k (Fig. 2A) and in Plasma 118k (Figure 2B) samples, while ApoB resulted enriched in fraction 4 and 5 for Plasma 118k preparation, and slightly present in fraction 6 and 7 in Plasma 16k preparation. Differences in lipoprotein distribution in gradient fractions could be due to donor to donor variations. On the other hand, both Plasma 16k and Plasma 118k fractions from 6 to 9 (corresponding to a density of 1.13-1.29 g/cm^3) resulted enriched in EV markers but depleted of blood contaminants such as lipoproteins and hemoglobin A (Supplementary Figure 2-9). Plasma samples showed weak signals from markers of the intracellular compartments GM130 and Calnexin, and only in fraction 6 (Fig. 2A, B).

Similarly, fractions 6 to 9 of Tissue 16k (Figure 3A) and Tissue 118k (Figure 3B) samples, after DSG processing, resulted enriched in EV markers and in SkM-EV markers. The SkM-EV marker Caveolin-3 was not detectable in plasma samples (Fig.2A,B), indicating that, with this experimental conditions, this protein is a specific SkM-EV marker[10,12,48].

In addition, signal of lipoprotein markers and adipose tissue markers were not present in these fractions (Supplementary Figure 10-15), indicating a negligible blood and adipose tissue contaminants in the SkM tissue biopsies. Tissue samples retain some amount of cellular marker Calnexin[6,19] in fraction 6 to 9, even if with decreased band intensity in comparison to the tissue homogenate and in opposite tendency to the increased signal of EV markers. It is to note that, in our experimental conditions, the chemiluminescent signal of GM130 was not detectable neither in homogenates obtained from the SkM tissue before and after the enzymatic treatment, nor in the gradient fractions, indicating that probably this marker is unsuitable for determining the presence of intracellular contaminants in human muscle samples, unlike SkM tissue from other species[10] (Supplementary Figure 10-15).

According to the results described above, we decided to focus our attention to fractions from 6 to 9 (Figure 2 and 3, green box) for all four preparations: these fractions are enriched in EV markers and contain nanoparticle with the typical density of EVs[26,33,44,45]. We discarded fractions 4 and 5 (Figure 2, red box) that still contain EV markers, but have lower density and, especially in plasma samples, are also enriched in lipoprotein markers. For further analyses fractions 6-9 have been collected and analyzed as a unique sample and will be further referred as Plasma 16k fractions 6-9 post gradient (PL16kG), Plasma 118k fractions 6-9 post gradient (PL118kG), Tissue 16k fractions 6-9 post gradient (TS16kG), Tissue 118k fractions 6-9 post gradient (TS118kG).

Pure Tissue samples from exogenous protein contaminants have a higher protein yield than Plasma Samples

Preparations PL16kG, PL118kG, TS16kG, TS118kG were checked for their purity from exogenous protein contaminants (EPC) with the COlorimetric NANoplasmonic (CONAN) assay as previously described[36–38]. Serial dilutions (1:1, 1:10 and 1:100 in HPLC water) of the samples were analyzed: PL16kG and PL118kG (Fig. 4A) resulted with an AI% lower than 20% at the minimal dilution of the sample (1:1) and remained below the 20% (dotted line) even at higher dilutions, but with increasing AI%. This means that the samples are clean from any detectable EPC[33,38,49,50]. TS16kG and TS118kG (Fig.4B) presented an AI% higher than 20% at the dilution 1:1, while it decreased under the 20% with the serial dilution 1:10 and 1:100, meaning that the samples are pure from EPC, but a further dilution is needed to fall the AI below the 20% dotted line. These data indicate that Tissue samples are more concentrated in EVs than Plasma samples.

After the purity check with the CONAN assay we performed BCA and Bradford assays to determine the protein concentrations in the samples (very likely associated to EVs). In order to compare the protein yield of samples from SkM tissue and plasma, the concentration was normalized to one gram of starting material (1 ml of Plasma and 1 gr of Tissue). BCA and Bradford results were comparable and in accordance to CONAN results. Tissue samples presented a significant higher protein yield than Plasma samples both with 16kG and 118G preparations measured with BCA (Figure 4C). It is to note that for the Bradford assay, these highly purified with low yield samples challenged the assay sensitivity[1]. Consequently, the protein concentration exhibited wide SEM, especially in TS16kG and TS118kG, and in the case of the PL16kG sample, it was undetectable (Figure 4D). However, despite these challenges, the trend of higher protein yield in Tissue samples compared to Plasma samples persisted, as indicated by BCA measurements.

Tissue and Plasma EV-enriched fractions display heterogeneous nanomechanical properties.

The morphology and nanomechanical characteristics of nanoparticles present in PL16kG, PL118kG, TS16kG and TS118kG preparations were evaluated using a high-throughput AFM imaging approach described[39,51] previously. Preliminary qualitative inspection of the resulting AFM micrographs revealed that all samples contained abundant globular particles with a morphology broadly compatible with that typically displayed by EVs (Fig. 5A,B,C,D).

We recently demonstrated that quantitative AFM morphometry can discriminate different subpopulations of nanoparticles in the same preparation on the basis of their nanomechanical properties. In particular, the stiffness of individual putative vesicles adhered to the substrate can be estimated via their equivalent spherical cap contact angle (CA). In samples derived from plasma, this technique was shown to discriminate EVs from NVEPs such as lipoproteins[40]. Briefly, since CAs were shown to be heavily influenced by the nanomechanical properties of their parent particle (*e.g.* the stiffness of intact EVs), collecting the morphometric measurements of individual objects from the same sample on a CA versus D plot results in the clustering of different subtypes of EVs and NVPs in specific zones of the plot[40].

Accordingly, the CA and D values of several hundred individual particles from PL16kG, PL118kG, TS16kG and TS118kG preparations were collected to evaluate the particle heterogeneity of each sample (Fig.5). All samples exhibited the typical log-normal distribution of sizes, containing abundant globular particles with D values below the range typically associated with intact EVs (<30 nm) and highly dispersed CA values surpassing those previously associated with lipoproteins (> 135°); although it is impossible to determine the biological identity of these particles via AFM, their CA and D ranges might be compatible with protein aggregates and/or other NVEPs. Given their higher stiffness compared to liposomes, they could be protein-enriched NEVPs, similar to exomeres[43].

Their overall similarity notwithstanding, the main differences between the four samples are found in the relative abundance, size and stiffness of particles with diameters above 50 nm. As shown in Figure 5E, PL16kG was found to contain a large fraction of particles within typical CA and D ranges previously associated with intact EVs from a variety of sources[39,40,51] (blue box, CA=80°-130° and D>30nm). On the other hands, the regions with lower CA (<80 nm), ascribed to other biogenic nanoparticles such as lipoproteins, was practically devoid of particles, confirming results from WB. The corresponding PL118kG preparation (Figure 5F) also contained a rich population of EV-compatible particles and a marginal presence of particles with lower CA values. We then applied the same analytical procedure to TS16kG (Figure 5G) and TS118kG (Figure 5H) samples. Despite being very similar to the Plasma preparations with abundant particles within typical CA and D ranges previously associated with intact EVs (blue box), both TS16kG and TS118kG samples showed a higher abundance of softer particles (CA below 80°, below the blue box) in the fraction of sizes above 50 nm. This means that the EV subpopulations in the samples enriched from SkM tissue present a more heterogeneous CA than EVs enriched from Plasma.

In addition, as outlined in the methods section, particle surface density calculations from AFM images allow estimating relative particle concentrations across different samples. With this method, the concentration of EVs in samples enriched from tissue (TS16kG and TS118kG) was found to be on average 10^2 times higher than the corresponding preparations from PL16kG and PL118kG as suggested by CONAN, BCA and Bradford assays (Supplementary Table 1).

Tissue samples have higher particles concentration, broader size distribution and higher colloidal stability than Plasma samples.

Concerning particle concentration, NTA can be employed to quantify this parameter, even though the techniques described earlier provide an estimation of whether one sample is more concentrated than another. Indeed, NTA results confirmed the data from CONAN, protein quantification and AFM, indicating a significant higher particle yield in TS16kG samples than PL16kG samples and

TS118kG samples respect to PL1118kG samples. Also in this case, to facilitate the comparison of particle yield between Plasma and Tissue samples, data have been normalized to one gram of starting material (Fig. 6A).

Samples size distribution was determined with orthogonal techniques: NTA, DLS and AFM. Each method has its advantages and limits and the combined evaluation of data obtained with different approaches allows to reveals different aspect and characteristics.

The size of particles was analyzed using NTA and mean size distribution profiles of preparations are shown in Fig. 6B. Both TS16kG and TS118kG samples have a broader size distribution than PL16kG and PL118kG respectively, with presence of EVs in the range from 30-200 nm, from 200 to 400 nm and also from 400 to 600 nm, while the majority of EVs from Plasma samples are in the range from 30-200 and 200-400 nm (Figure 6B). The mode size was found to be significantly different from TS16kG and PL16kG samples, with TS16kG EVs diameter larger than PL16kG EVs (166 ± 4 nm and 131 ± 3 nm respectively, Fig. 6C) while no significant differences were found in the mode size of TS118kG and PL118kG preparations (148 ± 4 nm and PL118kG 143 ± 4 nm respectively, Fig. 6C). NTA results data indicated that in TS16kG preparation the mode size of EVs is significantly higher than TS118kG sample.

The Laplace inversion analysis using the CONTIN algorithm was applied to autocorrelation functions obtained through DLS for four preparations (PL16kG, PL118kG, TS16kG, and TS118kG, Fig. 7A,D,G,L) to determine the size distribution of the samples[52]. The DLS profiles show a polydisperse size distribution, likely arising from a combination of the scattering from single and aggregated EVs, as well as from the scattering from objects of similar refractive index (e.g., proteins). The scattered intensity-weighted size distribution, depicted in Fig. 7B,E,H,M, provides a reliable analysis without assuming the composition of different populations. The results indicated that PL16kG and TS16kG samples are characterized by the presence of objects ranging from hundreds of nanometers to micrometers in diameter. In contrast, PL118kG and TS118kG

preparations exhibit bi-modal size distributions with a small subpopulation (around 100nm) and larger aggregates (diameter > 400 nm). It should be noted that DLS technique inherently tends to overestimate the presence of larger objects compared to smaller ones. Therefore, a number-weighted distribution is also presented (Fig. 7C,F,I,N). In this scale the majority of the scattering objects are around 100 nm diameter. This observation is consistent with the presence of small objects such as EVs, as corroborated by results from NTA and AFM.

Size distributions obtained via AFM morphometry can be inferred from the abundance of individual particles along the horizontal (D) axis of plots if Fig. 5E-5H. While a direct quantitative comparison of sizes distributions obtained from AFM and NTA is often questionable, the general trends observed by both techniques coincide: both AFM and NTA attribute to TS16kG EVs a higher diameter mode than PL16kG EVs (Fig. 5G and 5E, respectively), while those of TS118kG and PL118kG did not differ significatively (Fig. 5H and 5F, respectively). AFM also attributes to TS16kG EVs (Fig. 5G, blue box) a more heterogeneous size distribution than PL16kG EVs (Fig. 5E, blue box), with more particles populating the area of diameter between 100 and 300 nm in TS16kG sample, while PL118kG and TS118kG EVs (Fig. 5F and 5H, respectively) seems to be more homogenous.

Finally, we analyzed the colloidal stability of the four preparations measuring the zeta-potential. All measurements were done in milliQ H_20. TS16kG presented a mean zeta potential of -34.2 mV, PL16kG -13.7mV, TS118kG -24.2 and PL118G -10.6mV (Fig. 8). Notably, differences in colloidal stability between Plasma and Tissue-EVs enriched samples emerged. Both PL16kG and PL118kG exhibited a significantly higher zeta-potential compared to TS16kG and TS118kG, suggesting lower stability. This disparity implies that plasma EVs may be more susceptible to interactions with other components circulating in blood (i.e. other biogenic entities such as lipoproteins) than EVs in the extracellular matrix of SkM tissue. It will be interesting to evaluate if this property is specific of

blood EVs at the moment of the secretion of if EVs acquired it during the stay in a such a complex biofluid.

In conclusion, our results showed, for the first time, different biochemical and biophysical characteristics of EVs-enriched samples from human SkM and plasma. The observed differences regarding the protein composition, nanomechanical properties, particle yield, size and colloidal stability are not biased by the separation method and thus we can confidently say that reflect specific characteristics of EVs-enriched samples from solid and liquid matrixes. This pose new questions in understanding the determinants of these differences: the cellular origin, the molecular composition, the complex interaction between EVs and the biological environment. The last point highlights the importance of considering, in this scenario, the role of the biomolecular corona, the extravesicular cargo of molecules adsorbed to EVs and influenced by the surrounding matrix. In addition, it will be interesting to compare the biophysical properties of EVs from different human tissues isolated with the same protocol to see if they are SkM tissue-specific or typical of all tissue derived EVs.

From a broader standpoint, researchers may directly assess these traits as pivotal factors in the discovery of biomarkers[53]. The characterization of EV biophysical properties could serve as diagnostic tools for various SkM pathological conditions, complementing traditional biomolecular markers.

Acknowledgements

We thank Dr. Federica Bono from the Dept. of Molecular and Translational Medicine of the University of Brescia for the Ultra-Turrax T25 basic (IKA-Werke) homogenizer.

References

1. Théry C, Kenneth WW, Aikawa E, Alcaraz MJ, Anderson JD, Andriantsitohaina R, et al. Minimal information for studies of extracellular vesicles 2018 (MISEV2018): a position statement of the International Society for Extracellular Vesicles and update of the MISEV2014 guidelines. *J Extracell Vesicles* 2018; **7** :1535750.
2. Li SRM, Man QW, Gao XM, Lin HMa, Wang JM, Su FCM, et al. Tissue-derived extracellular vesicles in cancers and non-cancer diseases: Present and future. Journal of Extracellular Vesicles 2021; **10**, e12175.
3. Zhi Z, Sun Q and Tang W. Research advances and challenges in tissue-derived extracellular vesicles. *Frontiers in Molecular Biosciences* 2022; **9**.
4. Gonzalez PR, Gauthier SA, Kumar A, Levy E. The Exosome Secretory Pathway Transports Amyloid Precursor Protein Carboxyl-terminal Fragments from the Cell into the Brain Extracellular Space*. *Journal of Biological Chemistry* 2012; **287**, 43108–43115.
5. Vella LJ, Scicluna BJ, Chengd L, Bawden EG, Mastersa CL, Seng CA, et al. A rigorous method to enrich for exosomes from brain tissue. *Journal of Extracellular Vesicles* 2017; **6**, 1348885.
6. Huang Y, Cheng L, Turchinovichd A, Mahairakif V, Troncosof JC, Pletnikovág O, et al. Influence of species and processing parameters on recovery and content of brain tissue-derived extracellular vesicles. *Journal of Extracellular Vesicles* 2020*;* **9**, 1785746.
7. Brenna S, Altmeppen HC, Mohammadi B, Rissiek B, Schlinka F, Ludewig P, et al. Characterization of brain-derived extracellular vesicles reveals changes in cellular origin after stroke and enrichment of the prion protein with a potential role in cellular uptake. *J Extracell Vesicles* 2020; **9**, 1809065.
8. Zhang Z, Yu K, You Y, Jiang P, Wu Z, DeTure MA, et al. Comprehensive characterization of human brain-derived extracellular vesicles using multiple isolation methods: Implications for diagnostic and therapeutic applications. *Journal of Extracellular Vesicles* 2023; **12**, 12358.

9. Gomes PA, Bodo C, Ortiz CN, Samiotaki M, Chen M, Soares Cunha C, et al. A novel isolation method for spontaneously released extracellular vesicles from brain tissue and its implications for stress-driven brain pathology. *Cell Communication and Signaling* 2023; **21**, 35.

10. Watanabea S, Sudo Y, Makino T, Kimurab S, Tomitab K, Noguchic M, et al. Skeletal muscle releases extracellular vesicles with distinct protein and microRNA signatures that function in the muscle microenvironment. *PNAS Nexus* 2022; **1**, :173.

11. Ismaeel A, Van Pelt DW, Hettinger ZR, Fu X, Richards CI, et al. Extracellular vesicle distribution and localization in skeletal muscle at rest and following disuse atrophy. *Skeletal Muscle* 2023; **13**, 6.

12. Matejovič A, Wakao S, Kitada M, Kushida Y, Dezawa M. Comparison of separation methods for tissue-derived extracellular vesicles in the liver, heart, and skeletal muscle. *FEBS Open Bio* 2021; **11**, 482–493.

13. Bagge RO, Berndtsson J, Urzì O, Lötvall J, Micaroni M, Crescitelli R. Three-dimensional reconstruction of interstitial extracellular vesicles in human liver as determined by electron tomography. *J Extracell Vesicles* 2023; **12**, e12380.

14. Jeurissen S, Vergauwen G, Van Deun J, Lapeireb L, Depoorter V, Miinalainen I, et al. The isolation of morphologically intact and biologically active extracellular vesicles from the secretome of cancer-associated adipose tissue. *Cell Adh Migr* 2017*;* **11**, 196–204.

15. Crewe C, Joffin N, Rutkowski JM, Kim M, Zhang F, Towler DA, et al. An Endothelial-to-Adipocyte Extracellular Vesicle Axis Governed by Metabolic State. *Cell* 2018*;* **175**, 695-708.e13.

16. Hurwitz SN, Olcese JM, Meckes DG. Extraction of Extracellular Vesicles from Whole Tissue. *J Vis Exp* 2019; **144**, 10.3791/59143.

17. Crescitelli R, Lässer C, Lötvall J. Isolation and characterization of extracellular vesicle subpopulations from tissues. *Nat Protoc* 2021 **16** :1548–1580.

18. Jang SC, Crescitelli R, Cvjetkovic A, Belgrano V, Bagge RO, Jang KS, et al. Mitochondrial protein enriched extracellular vesicles discovered in human melanoma tissues can be detected in patient plasma. *J Extracell Vesicles* 2019*;* **8** :1635420.
19. Crescitelli R, Filges S, Karimi N, Urzì O, Alonso-Agudo T, Ståhlberg A, et al. Extracellular vesicle DNA from human melanoma tissues contains cancer-specific mutations. *Frontiers in Cell and Developmental Biology* 2022*;* **10** :1028854
20. Abreu CM, Costa-Silva B, Reis RL, Kundu SC, Caballero D. Microfluidic platforms for extracellular vesicle isolation, analysis and therapy in cancer. *Lab Chip* 2022*;* **22** :1093–1125.
21. Jeon H, Kang SK, Jeon MSL, Kang, SK, Lee MS. Effects of different separation methods on the physical and functional properties of extracellular vesicles. *PLOS ONE* 2020; **15** :e0235793.
22. Paolini L, Zendrini A, Di Noto G, Busatto S, Lottini E, Radeghieri A, et al. Residual matrix from different separation techniques impacts exosome biological activity. *Sci Rep* 2016; **6** :23550.
23. Wolf M, Poupardin RW, Ebner-Peking P, Andrade AC, Blöchl C, Obermayer A, et al. A functional corona around extracellular vesicles enhances angiogenesis, skin regeneration and immunomodulation. *Journal of Extracellular Vesicles* 2022; **11** :e12207.
24. Mol EA, Goumans MJ, Doevendans PA, Sluijter JPG, Vader P. Higher functionality of extracellular vesicles isolated using size-exclusion chromatography compared to ultracentrifugation. *Nanomedicine: Nanotechnology, Biology and Medicine* 2017; **13** :2061–2065.
25. Paolini L, Monguió-Tortajada M, Costa M, Antenucci F, Barilani M, et al. Large□scale production of extracellular vesicles: Report on the “massivEVs” ISEV workshop. *Journal of Extracellular Biology* 2022; **1** :63.
26. Radeghieri A, Alacqua S, Zendrini A, Previcini V, Todaro F, Martini G, et al. Active antithrombin glycoforms are selectively physiosorbed on plasma extracellular vesicles. *Journal of Extracellular Biology* 2022; **1** :e57.

27. Rome S. Muscle and Adipose Tissue Communicate with Extracellular Vesicles. *Int J Mol Sci* 2022; **23** :7052.

28. Latronico N, Rasulo FA, Eikermann M, Piva S. Critical Illness Weakness, Polyneuropathy and Myopathy: Diagnosis, treatment, and long□term outcomes. *Crit Care* 2023; **27** :469.

29. Lad H, Saumur TM, Herridge MS, Dos Santos CC, Mathur S, Batt J, et al. Intensive Care Unit-Acquired Weakness: Not just Another Muscle Atrophying Condition. *Int J Mol Sci 2020;* **21** :7840.

30. Faria M, Björnmalm M, Thurecht KJ, Kent SJ1, Parton RG, Kavallaris M, et al. Minimum information reporting in bio-nano experimental literature. *Nat Nanotechnol* 2018*;* **13** :777–785.

31. Van Deun J, Mestdagh P, Agostinis P, Akay Ö, Anand S, Anckaert J, et al. EV-TRACK: transparent reporting and centralizing knowledge in extracellular vesicle research. *Nat Methods* 2017; **14** :228–232.

32. Lucien F, Gustafson D, Lenassi M, Li B, Teske JJ, Boilard E, et al. MIBlood-EV: Minimal information to enhance the quality and reproducibility of blood extracellular vesicle research. *Journal of Extracellular Vesicles* 2023; **12** :12385.

33. Grossi I, Radeghieri A, Paolini L, Porrini V, Pilotto A, Padovani A, et al. MicroRNA□34a□5p expression in the plasma and in its extracellular vesicle fractions in subjects with Parkinson's disease: An exploratory study. *Int J Mol Med* 2021; **47** :533–546.

34. Paolini L, Radeghieri A, Civini S, Caimi L, Ricotta D. The epsilon hinge-ear region regulates membrane localization of the AP-4 complex. *Traffic* 2011; **12** :1604–1619 (2011).

35. Alvisi G, Paolini L, Contarini A, Zambarda C, Di Antonio V, Colosini A, et al. Intersectin goes nuclear: secret life of an endocytic protein. *Biochemical Journal* 2018; **475** :1455–1472 (2018).

36. Musicò A, Zenatelli R, Romano M, Zendrini A, Alacqua S, Tassoni S, et al. Surface functionalization of extracellular vesicle nanoparticles with antibodies: a first study on the protein corona "variable". *Nanoscale Advances* 2023*;* **5** :4703–4717.

37. Maiolo D, Paolini L, Di Noto G, Zendrini A, Berti D, Bergese P, *et al*. Colorimetric nanoplasmonic assay to determine purity and titrate extracellular vesicles. *Anal Chem* 2015*;* **87** :4168–4176.

38. Zendrini A, Paolini L, Busatto S, Radeghieri A, Romano M, Wauben MHM, et al. Augmented COlorimetric NANoplasmonic (CONAN) Method for Grading Purity and Determine Concentration of EV Microliter Volume Solutions. *Frontiers in Bioengineering and Biotechnology* 2020; **7** :452.

39. Ridolfi A, Brucale M, Montis C, Caselli L, Paolini L, Borup A, et al. AFM-Based High-Throughput Nanomechanical Screening of Single Extracellular Vesicles. *Anal. Chem.*2020; **92**, :10274–10282.

40. Ridolfi A, Conti L, Brucale M, Frigerio R, Cardellini J, Musicò A, et al. Particle profiling of EV-lipoprotein mixtures by AFM nanomechanical imaging. *Journal of Extracellular Vesicles* 2023; **12** :12349.

41. Nečas D, Klapetek P. Gwyddion: an open-source software for SPM data analysis. *Open Physics* 2012*;* **10** :181–188.

42. Busatto S, Zendrini A, Radeghieri A, Paolini L, Romano M, Presta M, et al. The nanostructured secretome. *Biomater. Sci. 2019;* **8** :39–63.

43. Zhang H, Freitas D, Kim HS, Fabijanic K, Li Z, Chen H, et al. Identification of distinct nanoparticles and subsets of extracellular vesicles by asymmetric flow field-flow fractionation. *Nat Cell Biol* 2018*;* **20**, 332–343.

44. Di Noto G, Paolini L, Zendrini A, Radeghieri A, Caimi L, Ricotta D. C-src Enriched Serum Microvesicles Are Generated in Malignant Plasma Cell Dyscrasia. *PLOS ONE* 2013; **8** :e70811.

45. Di Noto G, Chiarini M, Paolini L, Mazzoldi EL, Giustini V, Radeghieri A, et al. Immunoglobulin free light chains and GAGs mediate Multiple Myeloma Extracellular Vesicles uptake and secondary NfkB nuclear translocation. *Frontiers in Immunology 2014;* **5** :517.

46. Jeppesen, DK, Zhang, Q, Franklin JL, Coffey RJ. Extracellular vesicles and nanoparticles: emerging complexities. *Trends in Cell Biology* 2023; **33** :667–68.

47. Yamamoto T, Yamamoto A, Watanabe M, Matsuo T, Yamazaki N, Kataoka M, et al. Classification of FABP isoforms and tissues based on quantitative evaluation of transcript levels of these isoforms in various rat tissues. *Biotechnol Lett* 2009; **31** :1695–170.

48. Guescini M, Canonico B, Lucertini F, Maggio S, Annibalini G, Barbieri E, et al. Muscle Releases Alpha-Sarcoglycan Positive Extracellular Vesicles Carrying miRNAs in the Bloodstream. *PLOS ONE* 2015; **10** :e0125094.

49. Paolini L, Federici S, Consolia G, Arceria D, Radeghieri A, Alessandri I et al. Fourier-transform Infrared (FT-IR) spectroscopy fingerprints subpopulations of extracellular vesicles of different sizes and cellular origin. *Journal of Extracellular Vesicles* 2020; **9 :**1741174.

50. Mangolini V, Gualerzi A, Picciolini S, Rodà F, Del Prete A, Forleo L, et al. Biochemical Characterization of Human Salivary Extracellular Vesicles as a Valuable Source of Biomarkers. *Biology* 2023; **12** :227.

51. Borup A, Boysen AT, Ridolfi A, Brucale M, Valle F, Paolini L, et al. Comparison of separation methods for immunomodulatory extracellular vesicles from helminths. *Journal of Extracellular Biology* 2022; **1** :e41.

52. Montis C, Zendrini A, Valle F, Busatto S, Paolini L, Radeghieri A, et al. Size distribution of extracellular vesicles by optical correlation techniques. Colloids and Surfaces B: Biointerfaces. 2017; **1**; 158:331-338.

53. Paolini L, Zendrini A, Radeghieri A. Biophysical properties of extracellular vesicles in diagnostics. *Biomarkers in Medicine* 2017; **12** :0458.

Figure legends

Figure 1. Rationale of the paper sketched. Enrichment and characterization of EVs from human plasma and SkM tissue. After isolation, samples were characterized for their biochemical and biophysically properties. Created with Biorender.com.

Figure 2. Biochemical characterization of Plasma samples after sucrose gradient fractionation. Equal volume (20 μL) of each fraction both for Plasma 16k (A) and 118k (B) were loaded, 30 μg of Plasma total protein (PL). Samples were electrophoresed on SDS-PAGE gel (12% (Acrylamide/Bis-acrylamide) and analyzed for the antibodies described in the figures. Un-cropped WB are available in the Supplemental Material. Each fraction density is indicated in g/cm^3. Red box: fractions discarded for further analyses; Green box: fractions collected and further processed as a sample.

Figure 3. Biochemical characterization of Tissue samples after sucrose gradient fractionation. Equal volume (20 μL) of each fraction both for Tissue 16k (A) and 118k (B), 30 μg of Tissue Homogenate (TH) were loaded. WB for the antibodies described in the figures. Un-cropped WB are available in the Supplemental Material. Each fraction density is indicated in g/cm^3. The green box indicates fractions that, for further analyses, have been collected and further processed as a unique sample.

Figure 4. Purity assessment and protein concentration measurements.

Fractions 6 to 9 after the sucrose density gradient were collected and analyzed. Samples derived from Plasma (PL16kG, PL118kG) or Tissue (TS16kG, TS118kG). Samples were checked for purity from exogenous protein contaminants (EPC) with the CONAN assay. Aggregation Index ratios (AI%) of serial dilution (1:10, 1:100) of a representative sample are showed in the graph. The dotted line represents the CONAN assay threshold for EPC detection (AI% <20% EPC content ≤0.05 μg/μl). The AI% is inversely proportional to the preparation purity and samples with AI% below the 20% are considered pure. AI% values of a representative sample with assay internal controls (NormREF, black dots; IntREF, green dots) (A); Protein concentration with BCA (B) and

Bradford assay (C); Protein concentration for each group was normalized by tissue mass (per 1 gr). Values were shown as mean ± SEM. Significant differences among datasets were determined with Student's t-test. P values: ****p < 0.0001. TS16kG, dark blue points; PL16kG, dark red squares; TS118kG, light triangle up; PL118kG, light red triangle down.

Figure 5. Nano-mechanical features of samples from Plasma and Tissue**.** Representative AFM images of PL16kG (A), PL118kG (B), TS16kG (C), and TS118kG (D). Contact angle VS diameter plot of several hundred individual particles from at least five different depositions for each sample as calculated via AFM morphometry of PL16kG (E), PL118kG (F), TS16kG (G) and TS118kG (H). Blue box represents area populated by structures with the typical EV-like characteristics: contact angle ranging from 75° to 135°, diameter from 30 to 300 nm.

Figure 6. Concentration and size distribution. Particle concentration for each sample were measured by NTA. Particle concentration was normalized for starting material mass (1gr) (A). Particle Size distribution was measured by NTA. Histograms represent the mean of the size distribution divided by range (0-200 nm; 200-400 nm; 400-600 nm) of the 16k and 118k samples from plasma and tissueB). Particle size was analyzed by NTA and modal distribution (nm) (C). Values in nm were shown as mean ± SEM. Significant differences among datasets were determined with Student's t-test. P values: **p< 0.01, ***p < 0.001 and ****p < 0.0001.

Figure 7. Size distribution with DLS. Representative autocorrelation function of the scattered intensity, with the fitting curve according to the Laplace Inversion via CONTIN algorithm (A,D,G,L); corresponding scattered intensity-weighted (B,E,H,M) and number-weighted (C,F,I,N) size distributions of scattering objects of samples described in the text.

Figure 8. Zeta-potential measurement. Preparations were analyzed for their colloidal stability measuring z-potential with DLS. Values in mV were shown as mean ± standard error of the mean (SEM). Significant differences among datasets were determined with Student's t-test. P values: **p< 0.01.

Authors' Contributions

CRediT taxonomy. VM Data curation, Formal analysis, Investigation, Methodology, Writing - review & editing; AR Conceptualization, Data curation, Formal analysis, Investigation, Funding acquisition, Writing - review & editing; SP Conceptualization, Data curation, Formal analysis, Funding acquisition, Writing - review & editing; SC Investigation, Methodology, Writing - review & editing; NL Conceptualization; Data curation; Formal analysis; Funding acquisition, Writing - review & editing; MB Investigation, Methodology, Data curation, Writing - review & editing; FV Investigation, Methodology, Data curation; AB Investigation, Methodology, Writing - review & editing; CM Investigation, Methodology, Writing - review & editing; PB Conceptualization; Data curation; Formal analysis; Funding acquisition, Writing - review & editing; LP Conceptualization, Data curation, Formal analysis, Funding acquisition, Investigation; Methodology, Writing - original draft

Availability of Data and Materials

Raw data from CONAN and DLS data of all samples analyzed are available on Zenodo repository link https://doi.org/10.5281/zenodo.10579305

Supplementary Materials

Supplementary materials are available.

Ethical Approval and Consent to Participate

Research was conducted in accordance in accordance with The Code of Ethics of the World Medical Association (Declaration of Helsinki) and Good Clinical Practice. The study was approved by the ethics committee of Spedali Civili di Brescia (Protocol number 3468). Informed consent was obtained from all the subjects enrolled in the study. The privacy rights of subjects involved in the study have always been observed.

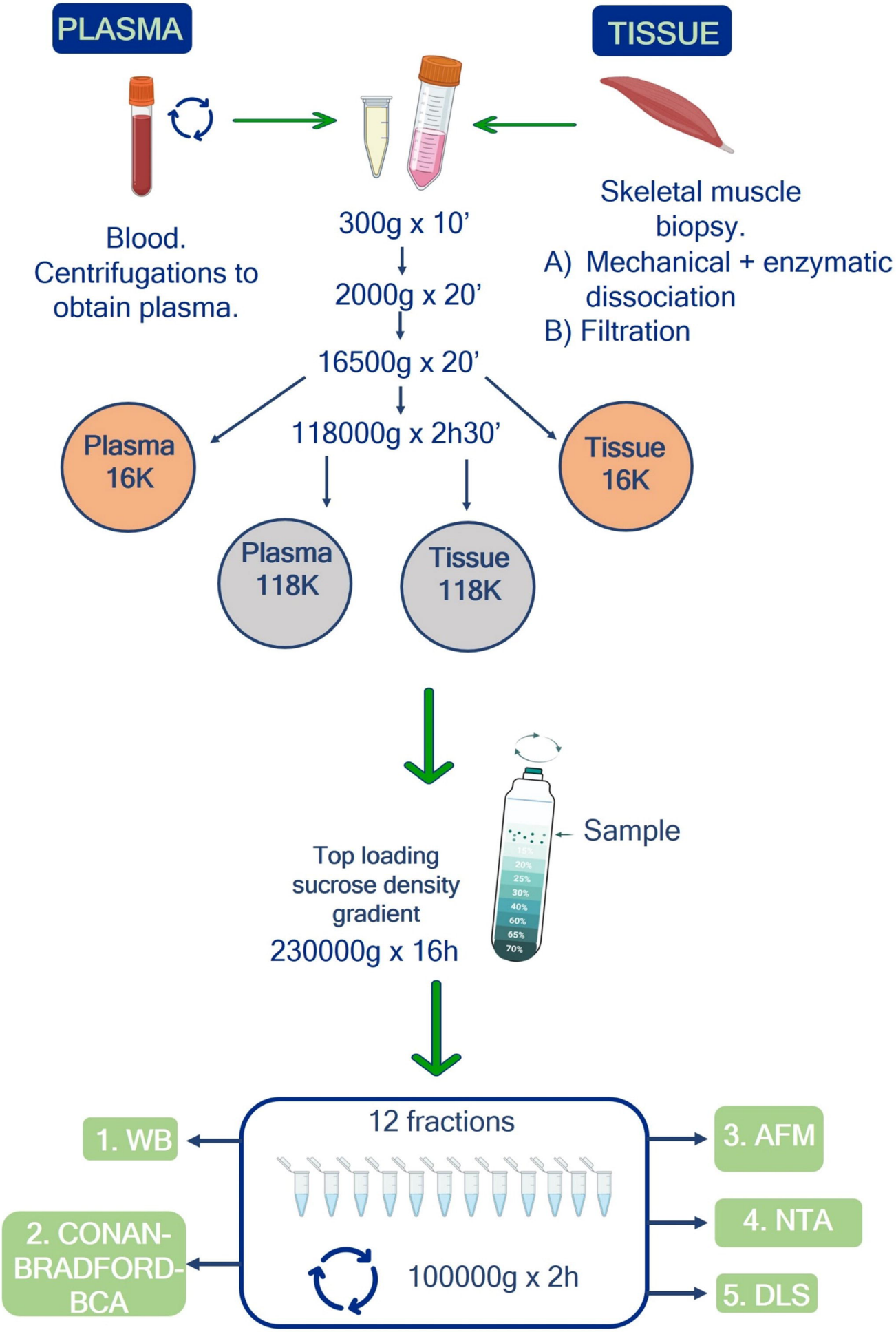
PLASMA
TISSUE
Blood.
Centrifugations to obtain plasma.
300g x 10'
2000g x 20'
16500g x 20'
118000g x 2h30'
Skeletal muscle biopsy.
A) Mechanical + enzymatic dissociation
B) Filtration
Plasma 16K
Plasma 118K
Tissue 118K
Tissue 16K
Sample
Top loading sucrose density gradient
230000g x 16h
12 fractions
100000g x 2h
1. WB
2. CONAN-BRADFORD-BCA
3. AFM
4. NTA
5. DLS

A) Plasma 16K

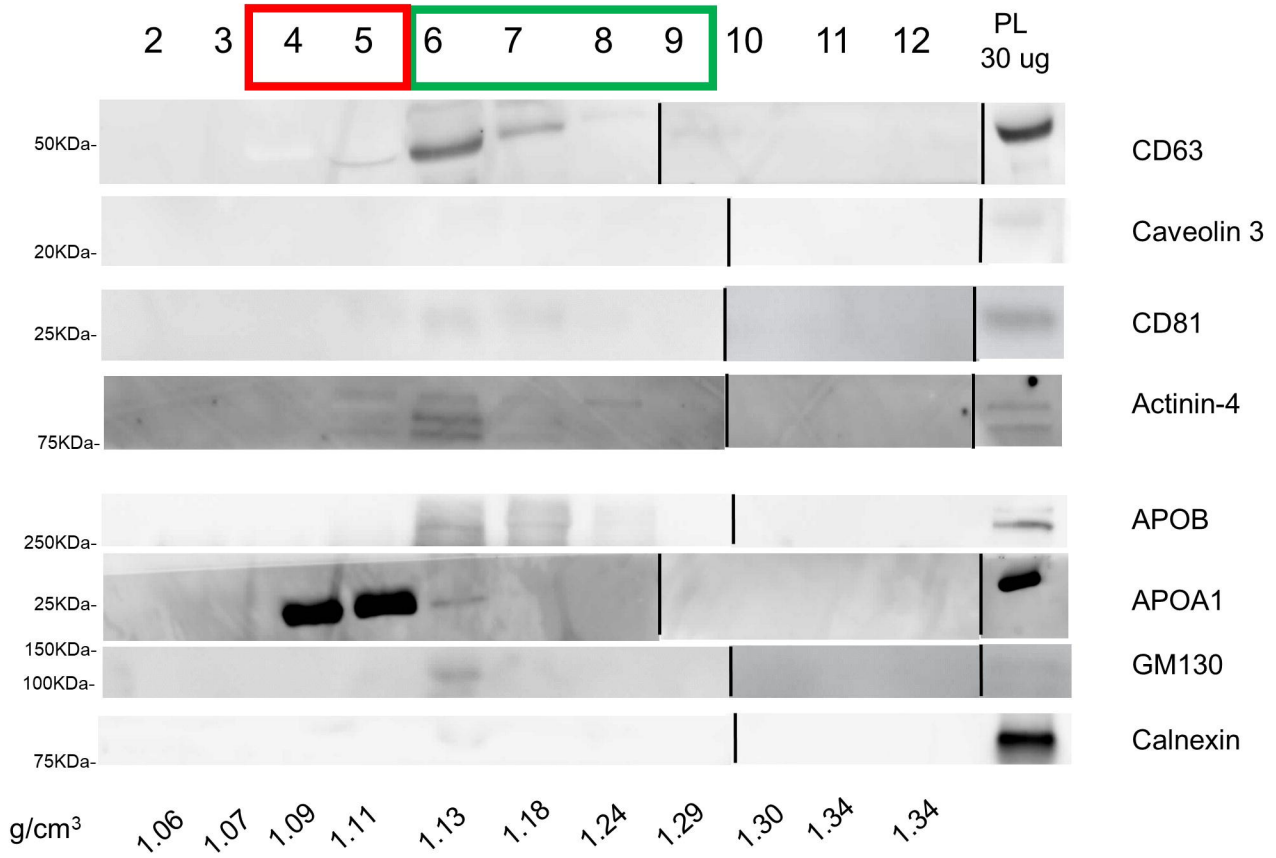

B) Plasma 118K

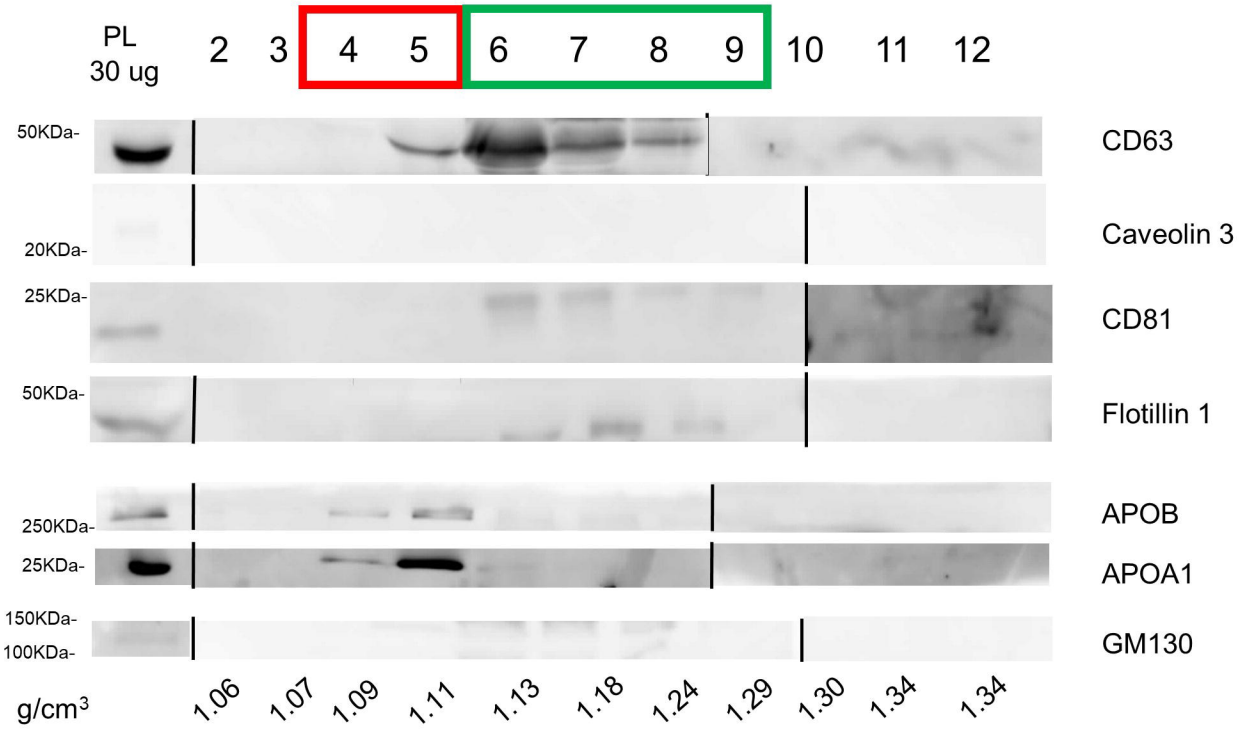

A) Tissue 16K

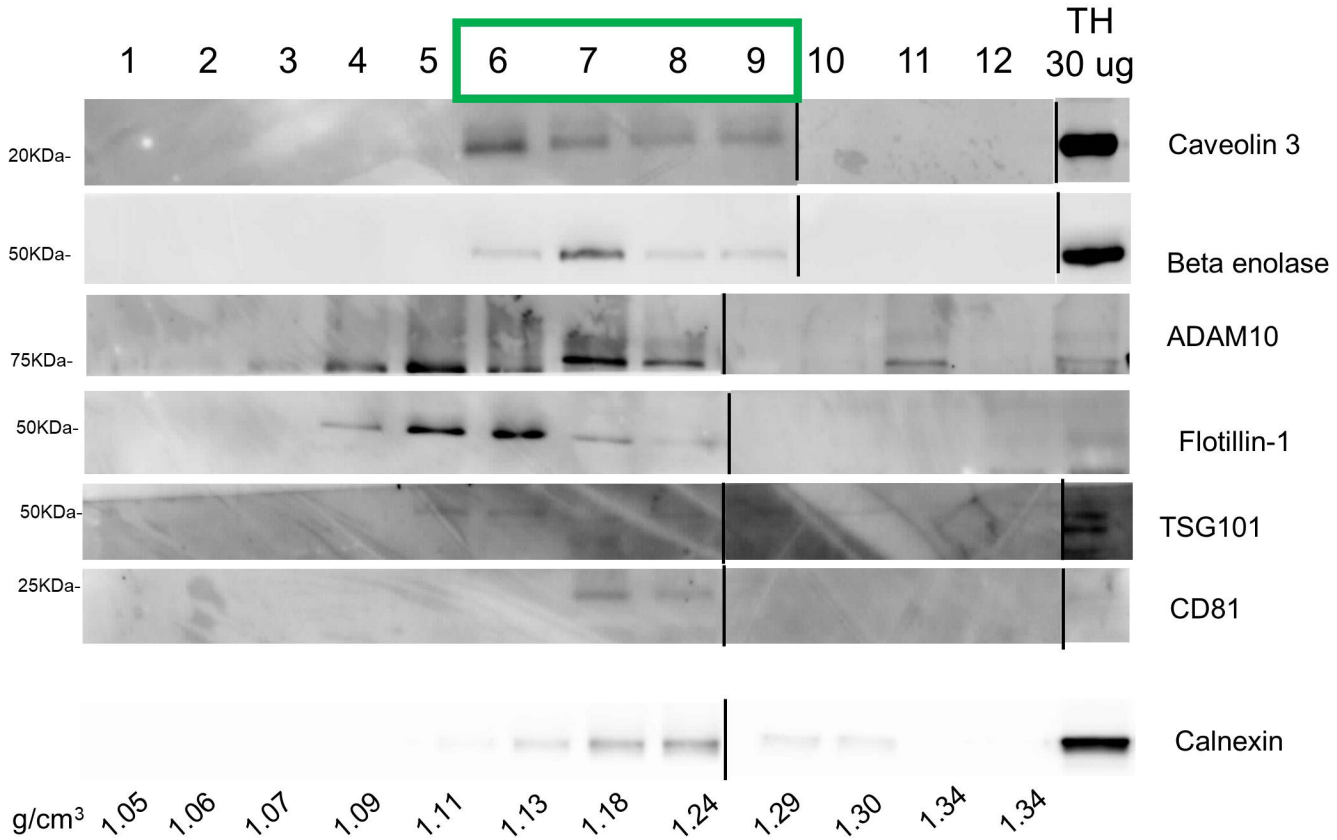

B) Tissue 118K

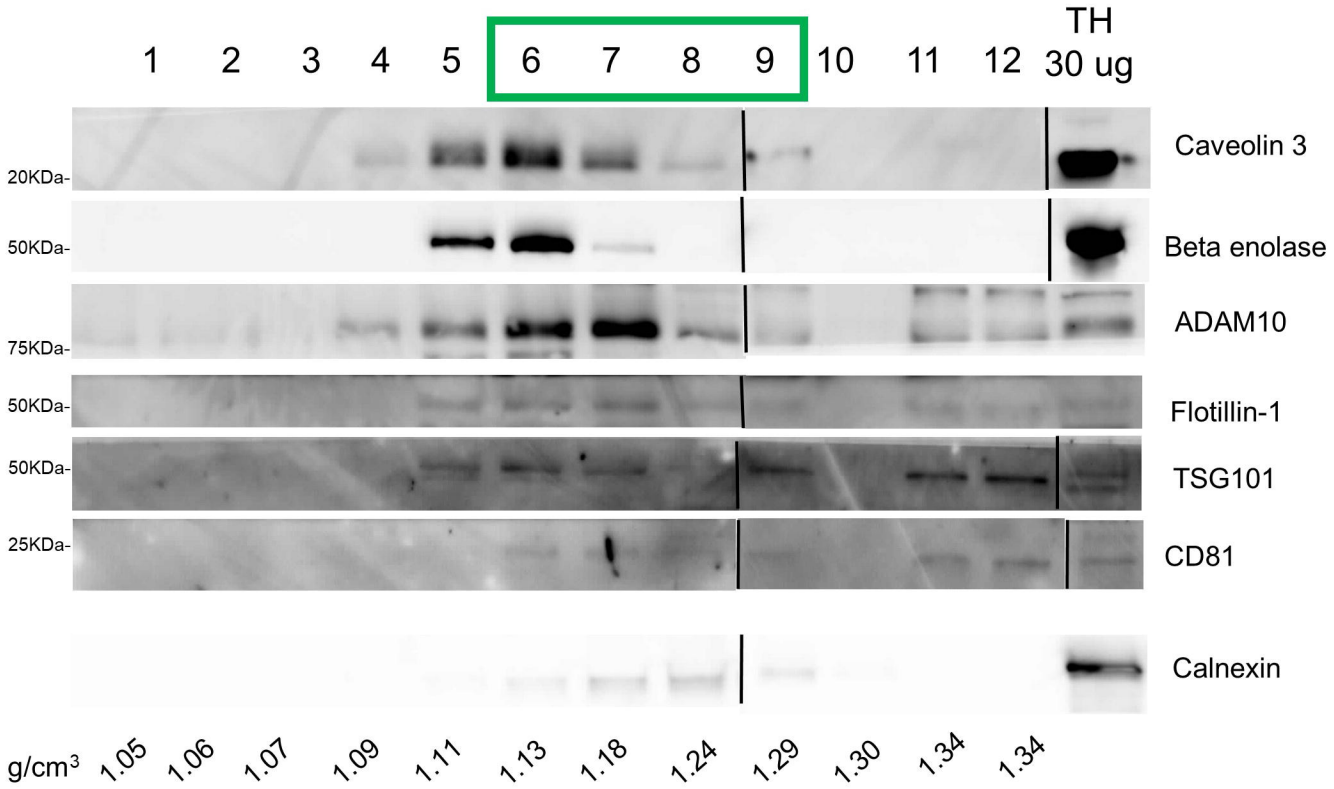

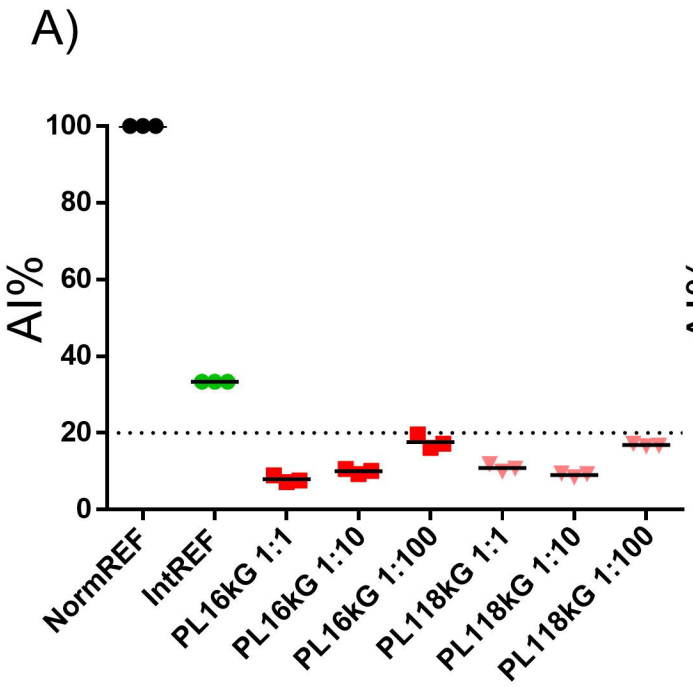
A)
AI%
100
80
60
40
20
0
NormREF
IntREF
PL16kG 1:1
PL16kG 1:10
PL16kG 1:100
PL118kG 1:1
PL118kG 1:10
PL118kG 1:100

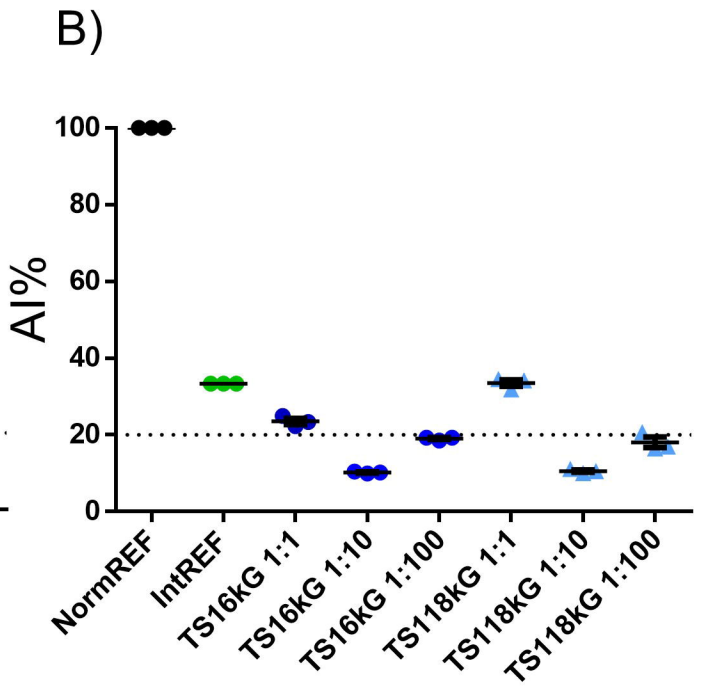
B)
AI%
100
80
60
40
20
0
NormREF
IntREF
TS16kG 1:1
TS16kG 1:10
TS16kG 1:100
TS118kG 1:1
TS118kG 1:10
TS118kG 1:100

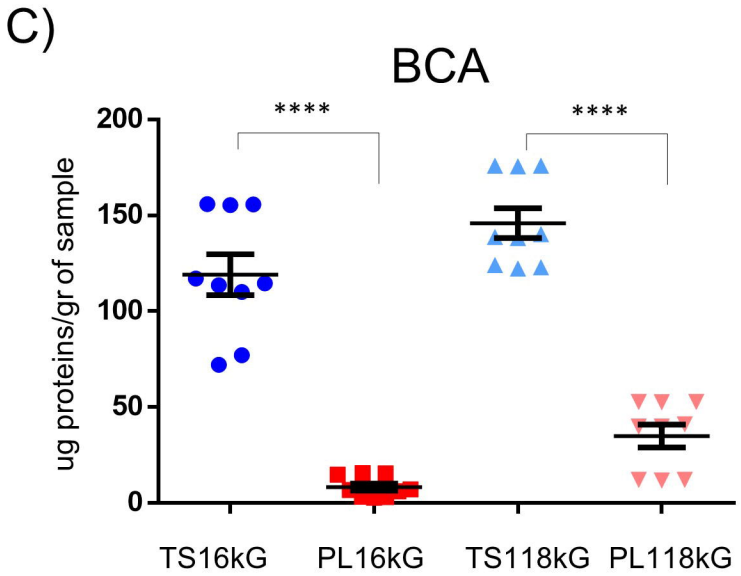
C)
BCA
****
****
ug proteins/gr of sample
200
150
100
50
0
TS16kG
PL16kG
TS118kG
PL118kG

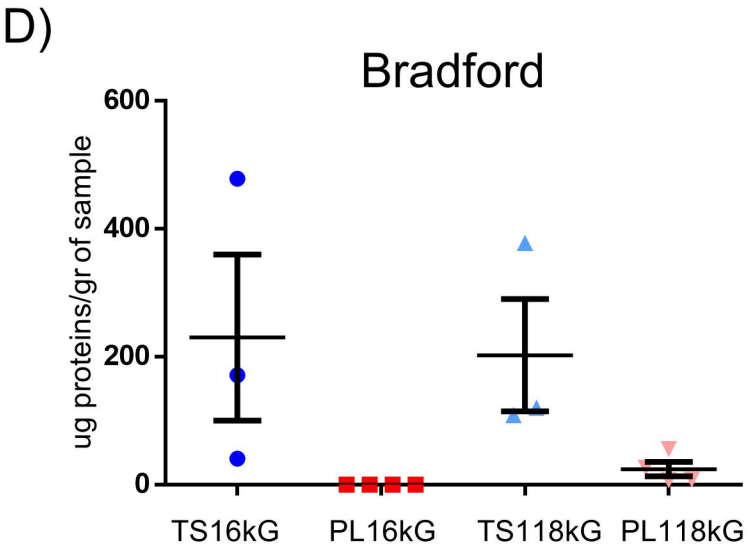
D)
Bradford
ug proteins/gr of sample
600
400
200
0
TS16kG
PL16kG
TS118kG
PL118kG

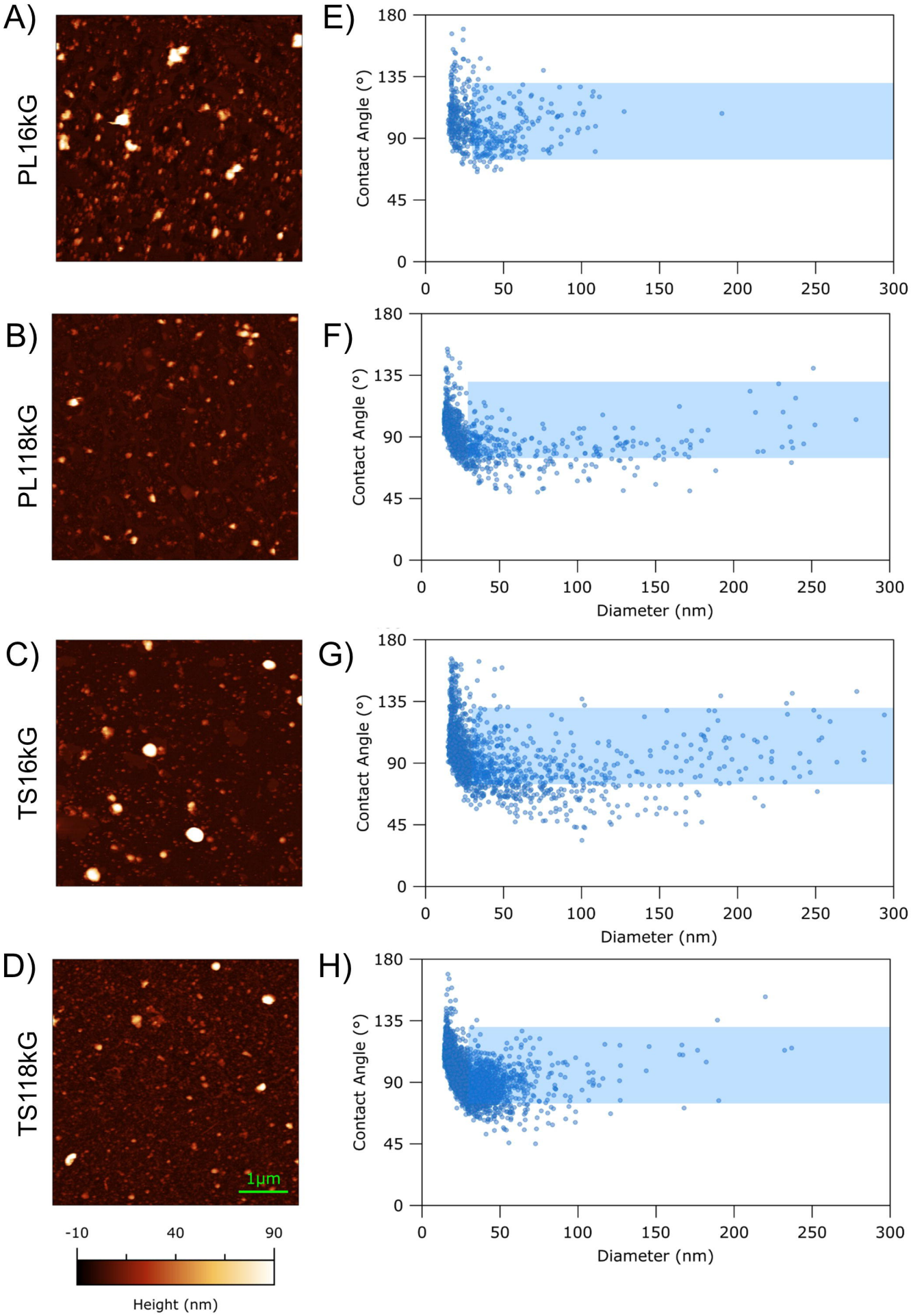
A)
PL16kG
B)
PL118kG
C)
TS16kG
D)
TS118kG
1µm
-10
40
90
Height (nm)
E)
F)
G)
H)
Contact Angle (°)
Diameter (nm)
0
45
90
135
180
0
50
100
150
200
250
300

A)

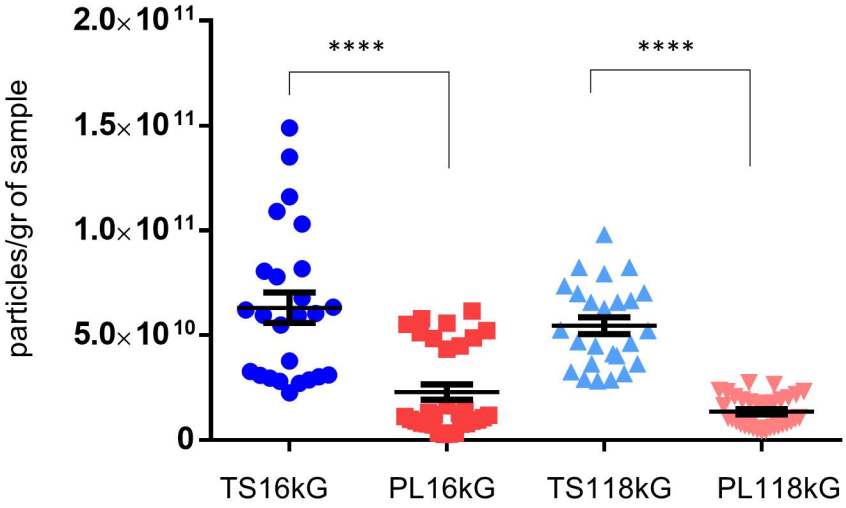
particles/gr of sample
2.0×10 11
1.5×10 11
1.0×10 11
5.0×10 10
0
****
****
TS16kG
PL16kG
TS118kG
PL118kG

B)

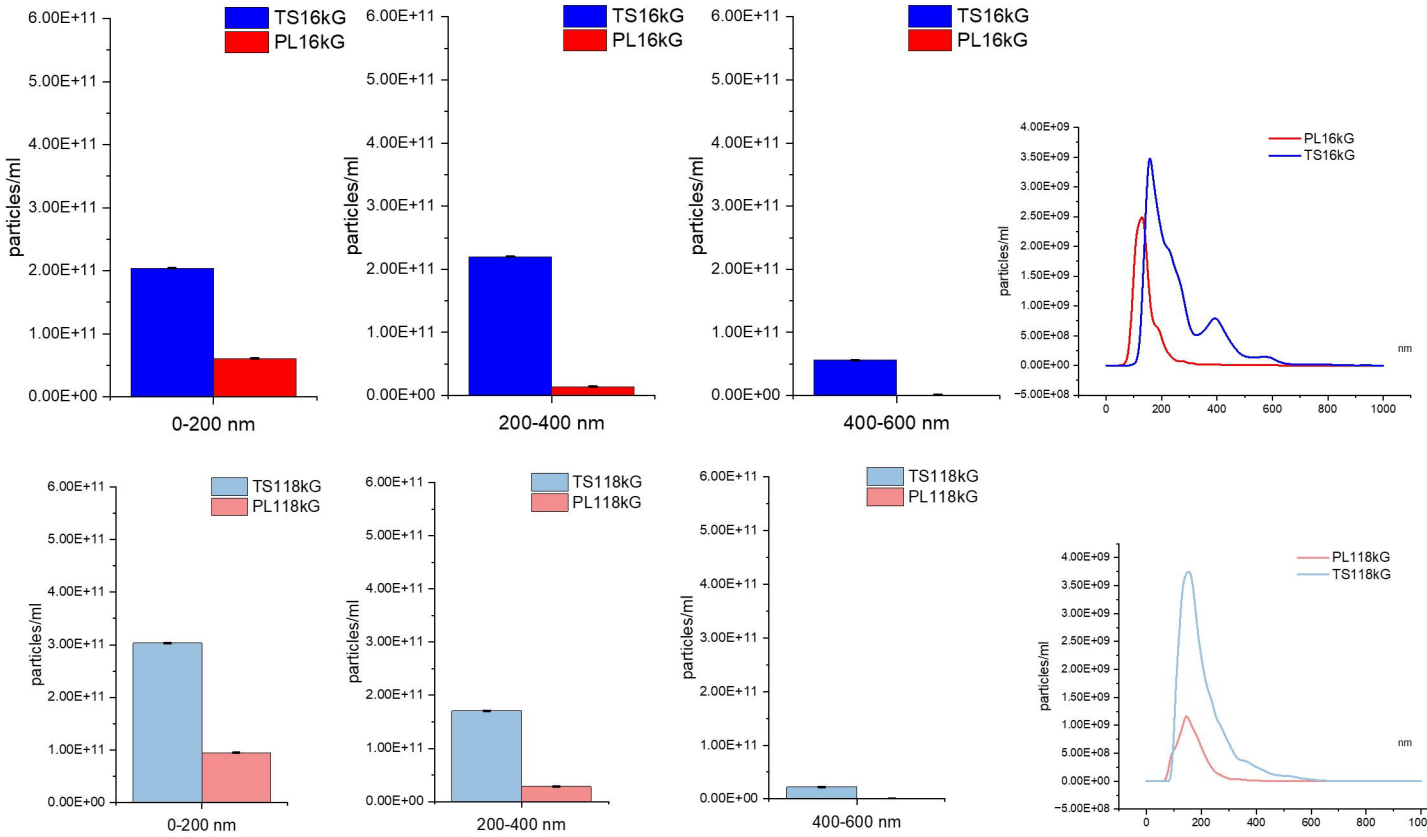
TS16kG
PL16kG
particles/ml
0-200 nm
200-400 nm
400-600 nm
PL16kG
TS16kG
nm
TS118kG
PL118kG
PL118kG
TS118kG

C)

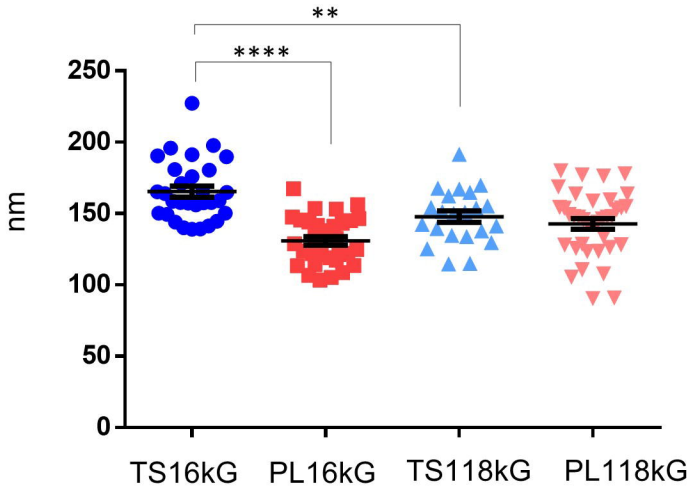
nm
250
200
150
100
50
0
**
****
TS16kG
PL16kG
TS118kG
PL118kG

PL16kG

A)

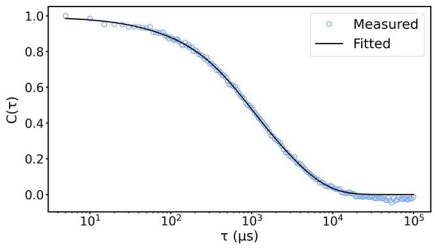

B)

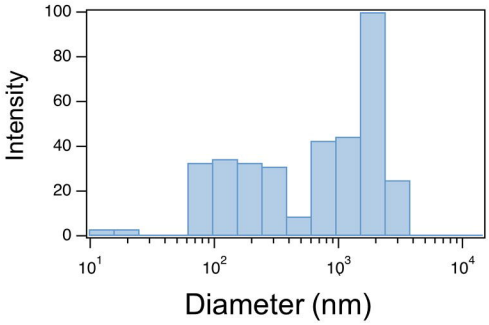

C)

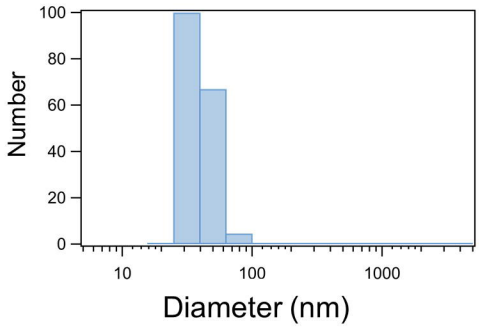

PL118kG

D)

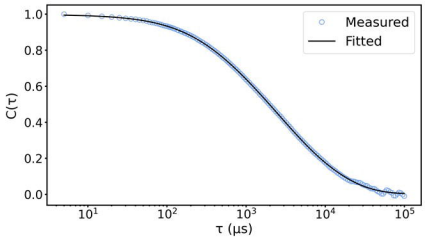

E)

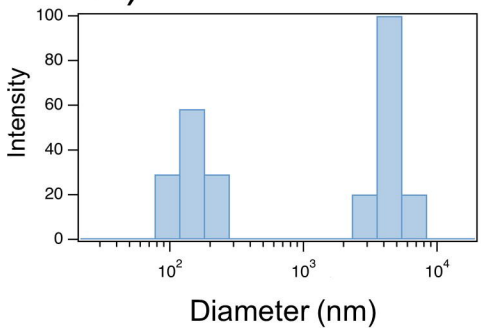

F)

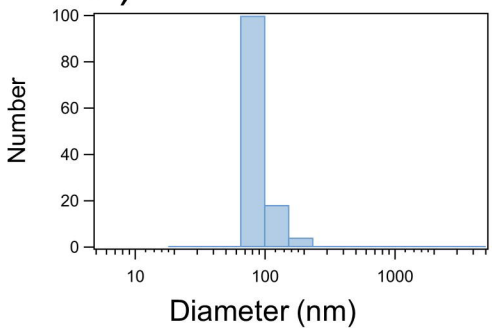

TS16kG

G)

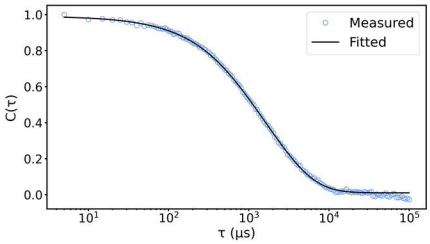

H)

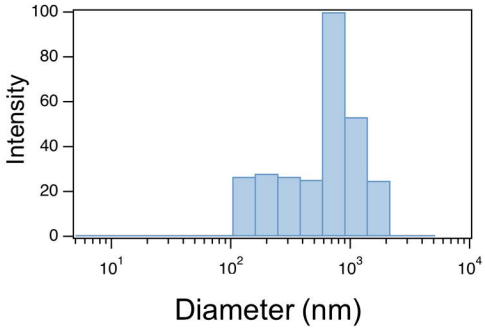

I)

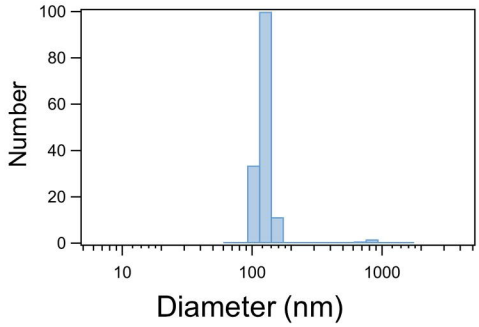

TS118kG

L)

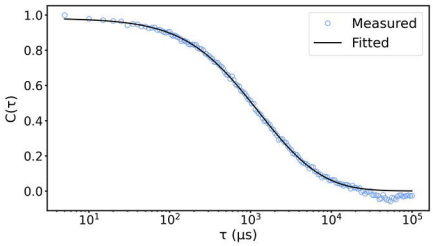

M)

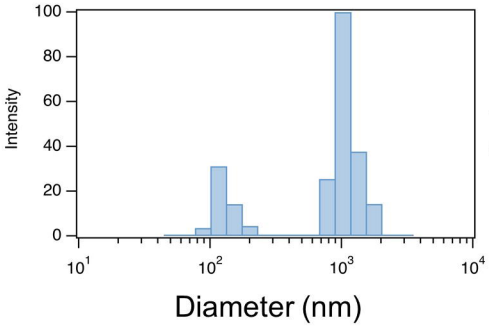

N)

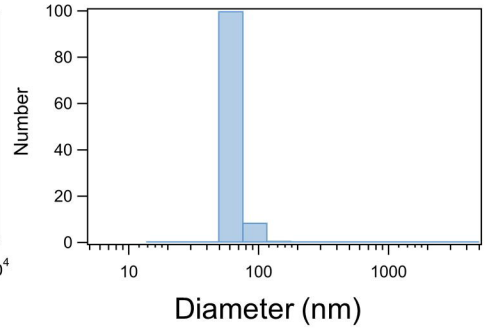

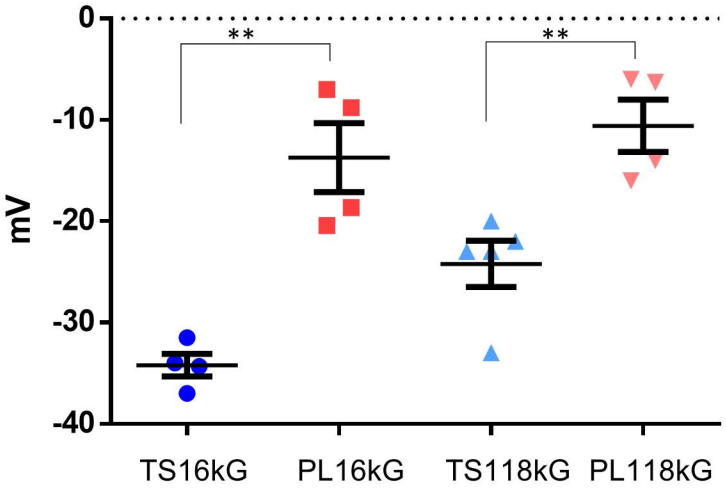
0
-10
-20
-30
-40
mV
**
**
TS16kG
PL16kG
TS118kG
PL118kG

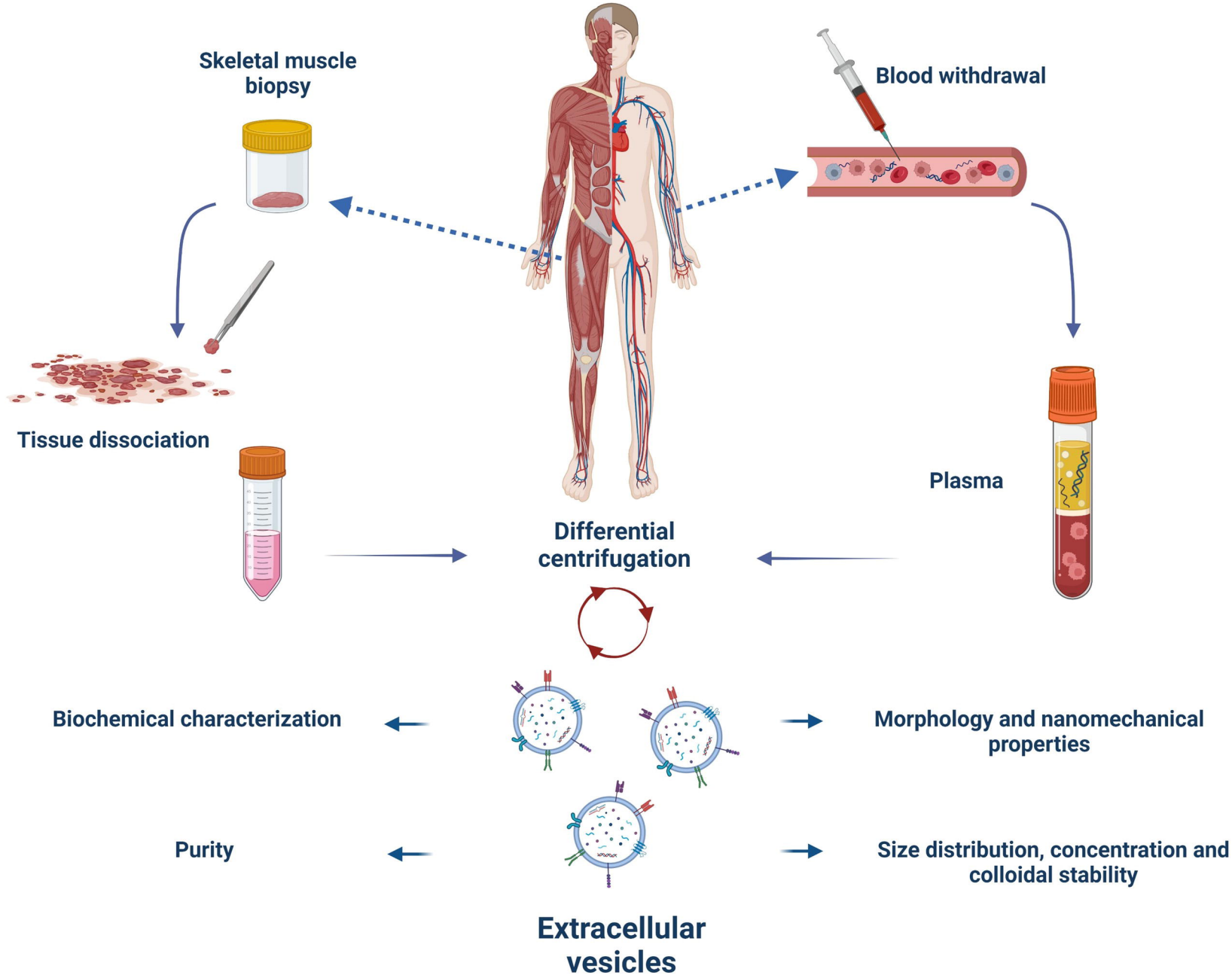
Skeletal muscle biopsy
Blood withdrawal
Tissue dissociation
Plasma
Differential centrifugation
Biochemical characterization
Morphology and nanomechanical properties
Purity
Size distribution, concentration and colloidal stability
Extracellular vesicles